IEEE Access
Multidisciplinary ⋮ Rapid Review ⋮ Open Access Journal

Received 13 August 2023, accepted 21 August 2023, date of publication 25 August 2023, date of current version 5 September 2023.

Digital Object Identifier 10.1109/ACCESS.2023.3308827

RESEARCH ARTICLE

Research on Motion Control of Bionic Sucker Inchworm Robot Based on MPC

CHENGZE XUE, QIAOLING DU, WENLI MA, AND YINFENG GENG
State Key Laboratory on Integrated Optoelectronics, College of Electronic Science and Engineering, Jilin University, Changchun 130012, China
Corresponding author: Qiaoling Du (duql@jlu.edu.cn)

This work was supported in part by Jilin Province Science and Technology Development Plan Project under Grant 20190303008SF.

ABSTRACT Inchworm robots are typical insect bionic robots that are able to move in narrow space such as pipelines, which expand the range of robot application. In this paper, the motion control method of the bionic sucker inchworm robot (BSIR) based on MPC is proposed, which enables the inchworm robot to achieve "Ω" motion gait and steering gait on vertical and horizontal planes of different materials. Firstly, the negative pressure suction cup imitating octopus tentacles (NPSC-IOT) is designed and the sucker control model is proposed. Under negative pressure control, the adsorption pressure of the sucker is adjusted to satisfy the needs of the trunk structure movement. Secondly, the bionic sucker controller based on MPC is designed, and the closed-loop control is realized by using the data feedback from the air pressure sensor. Thirdly, BSIR with installed NPSC-IOT as the robot's tentacles is developed. Finally, the experiment verifies the feasibility of the bionic sucker controller based on MPC to control BSIR to achieve 'Ω' motion gait and steering gait on vertical and horizontal planes of different materials. The experimental results show that BSIR is able to achieve "Ω" gait and turning gait on vertical and horizontal surfaces of glass, tiles, white gray walls, and metal.

INDEX TERMS Bionic octopus sucker, bionic inchworm, MPC control, crawling robot, motion planning.

I. INTRODUCTION

Bionic robots are the important branch of robot field. The current application of bionic robots has realized the imitation of part of the structure and function of human or animal in nature [1] or motion characteristics [2]. The bionic robots that have been realized in the current research include bionic mechanical fish, bionic hexapod robot, bionic flapping wing machine, mechanical gecko and mechanical frog. However, in some special environments, such as the detection of industrial environment, the search and rescue of earthquake site and the exploration of transmission pipeline, the conventional bionic robot [3] can't walk normally in this area, so that it can't complete the tasks of detection, search and rescue. In order to solve such problems, researchers have focused on insects that are able to move in the small space, and studied the use of bionic technology to achieve the movement of such robots to meet the special needs of industrial sites. Aiming at the robot moving in special environment, this paper studies the key technology of the bionic sucker inchworm robot (BSIR) motion based on MPC control method.

As the bionic insect robot, the inchworm robot has attracted the attention of many researchers. The composition and control of the body structure of the inchworm robot is one of the key technologies to realize multi-degree-of-freedom control. The torso body of the inchworm robot currently studied usually adopts an Ω-shaped mechanical structure [4]. For example, the structure of the Omegabot crawling robot achieved the functions of extension and contraction. The torso structure of such robots was composed of multiple 1-DOF (Degrees Of Freedom) motion joints in series, eliminating other redundant structures and retaining functional structures [5], [6]. This control method was similar to the single-legged control of multi-legged robots [7]. Compared with multi-legged robots, it shows simple and efficient advantages in both mechanical and control aspects [8], [9], [10]. In order to further simulate the peristaltic movement of the inchworm, researchers from Virginia Tech University improved and designed the millipede robot, adding a large number of gastropods to its trunk structure, which made the robot move through the swing of

The associate editor coordinating the review of this manuscript and approving it for publication was Okyay Kaynak.

This work is licensed under a Creative Commons Attribution-NonCommercial-NoDerivatives 4.0 License.
For more information, see https://creativecommons.org/licenses/by-nc-nd/4.0/

the abdominal foot [11], [12]. Researchers from the Central Institute of Mechanical Engineering in India have created a large number of joints in the torso, allowing the robot to move through the swinging friction of the joints [13]. In addition, the connecting rod robot designed by Hanyang University in South Korea and the double anchor crawling robot designed by the University of Texas in the United States made the trunk composed of two motion joints, which performed 1-DOF reciprocating motion over short distance and had the lowest peristaltic motion performance [14], [15].

With the emergence of various new materials, the researchers used the soft structure to construct the torso structure of the inchworm robot. Researchers at Beijing University of Aeronautics and Astronautics used memory alloy to simulate the trunk of the inchworm robot, and electronically controlled the elasticity of the memory alloy to simulate the crawling movement of caterpillars, completing the crawling motion [16]. The trunk of the modular soft robot and the double finger gripper robot designed by researchers from Tianjin University was composed of pneumatic actuators. This structure was composed of soft material elements to form the small strain angle module, and then the plurality of modules were combined to form a large deformation bending of the overall structure [17]. The lightweight materials of these structures provided new ideas for the lightweight of robot structures, and the driving form was slightly different from the traditional driving [18], [19]. The rigidity of the soft material is small and the load-bearing is small, which limits the volume and operation ability of the robot, and the development cost of related materials is large. At present, the leg structure is used to replace the trunk part, and reducing the structural redundancy of the robot is the best choice to balance the cost and performance. From the perspective of control, the trunk is composed of servo motors, and its control process is simple and stable. Therefore, this paper studies the method of the bionic sucker control based on MPC to improve the bionic performance of this simple torso structure.

Another important structure of the inchworm body is the tentacles at both ends, which are the important force points during the movement of the inchworm. Therefore, the design and control of the structure are the key technologies for the inchworm robot to complete the movement in different environments. The tentacles of inchworm robots usually adopt claw structure, electromagnet foot structure and fine bristles structure. Most of the claw-type structures rely on the clamping rod structure to fix their own posture. For example, the climbing rod robot designed in our laboratory was able to complete the designated motion planning [20]. However, the claw structure was difficult to stabilize its posture as a force point, and its analysis and control process is relatively complex. Different from the structure of the mechanical claw, the electromagnet as the foot structure is able to adsorb the motion plane, which can provide a very stable force point for the robot, and the control process is relatively simple [21]. The soft toe electromagnetic foot module designed by researchers from Thailand can enable robots to move in various environments by improving the contact surface shape of the electromagnet [22]. However, the electromagnet foot structure is only suitable for adsorbing metals such as iron, nickel, and cobalt, which limits the materials used in robot motion scenarios. The biomimetic gecko robot designed by researchers at the National Institute of Science in South Korea and the wet adhesive pad designed by Tongji University simulated the tentacles of geckos or insect footpads by increasing foot contact surfaces. The foot contact surface of the gecko tentacle was designed with many small protrusions made of polyethylene siloxane material. Applying pressure on the foot, this structure and the contact plane produced the tangential van der Waals force, causing the two to adsorb together [9], [23], [24]. Due to the flexibility of the raised material and the substrate material, the adhesive stability of the structure itself was not high, and the foot size was also large, which posed a great challenge to its miniaturization process. Researchers studied the movement of octopuses and found that their adsorption movement was different from the first three forms. Octopuses use suction cups on their tentacles to fix their bodies on a moving surface and move by switching the tentacle attachment [25].This structure of the octopus sucker is beneficial to reduce the size of the foot structure. Therefore, this paper studies the negative pressure suction cup imitating octopus tentacles (NPSC-IOT) as the tentacle of the imitation inchworm robot.

This article draws inspiration from the body structures of two organisms, the inchworm and octopus, and some researchers have conducted in-depth research on them [26], [27], [28]. Since the trunk structure we designed adopts the connection drive structure of the traditional servo motor, we will use the mature forward and inverse kinematics analysis method [29] according to the structure model. Compared with the more complex flexible material structure, our control process will be simpler and more stable. For robots with unconventional structures, some researchers have focused on optimizing their gait [30], [31] to make their movements more accurate. But the demand for control accuracy in the robot motion we design is not high, and there is not only one posture that can complete the robot's motion. Therefore, we pay more attention to the gait planning of the robot and design more robot gait to adapt to the complexity of the environment. The diversity of gait can help robots choose suitable and effective gait for transition when facing environmental constraints.

In this paper, NPSC-IOT is designed, and the sucker control method based on MPC (Model Predictive Control) is proposed [33]. And BSIR is developed. The robot can achieve "Ω" motion gait and steering gait on vertical and horizontal planes of different materials. This expands the robot's mobile environment and increases its ability to adapt to the environment. The main contributions of this paper are as follows:

(1) NPSC-IOT is designed, and the sucker control model is proposed. By using this control method, the adsorption pressure of the sucker is adjusted to meet the needs of trunk structure movement.

(2) The bionic sucker controller based on MPC is designed. The closed-loop control is realized by the data feedback from the pressure sensor. The MPC control algorithm adjusts the suction force of the sucker by changing the flow rate of the vacuum pump.

(3) BSIR is developed. The NPSC-IOT is installed at the end of BSIR as the tentacles of the robot. Four longitudinal servo motors and two transverse servo motors are installed in its trunk structure, which can realize 'Ω' type movement gait and steering gait.

(4) The motion gait planning of MPC-BSC (Model Predictive Control-Bionic Sucker Control) is proposed, which controls BSIR to achieve "Ω" motion gait and steering gait on vertical and horizontal planes.

The remaining contents of this paper are as follows: The second part describes in detail the structural design of NPSC-IOT, the control model of the sucker and the control algorithm of the sucker force based on MPC. The third part introduces the structure of BSIR, and proposes the gait planning based on MPC-BSC. The fourth part describes NPSC-IOT test, MPC-BSC test and motion test based on MPC-BSC in detail, and analyzes the related performance. The fifth part summarizes the full text.

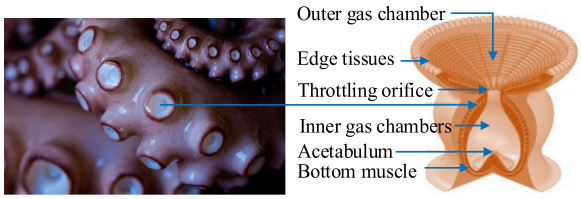

FIGURE 1. The sucker structure of octopus.

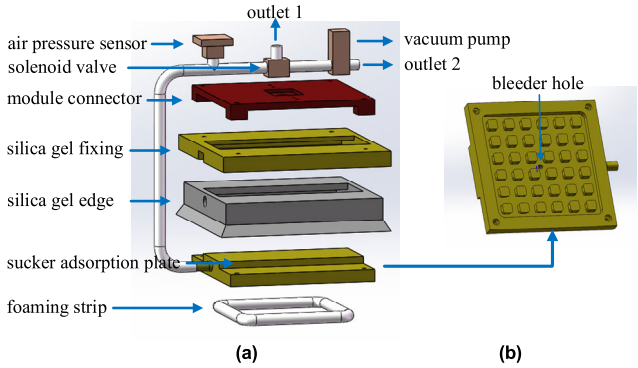

FIGURE 2. Sucker structure: (a) The structure decomposition of sucker (b) The contact surface structure of sucker adsorption plate.

II. BIONIC SUCKER CONTROLLER BASE ON MPC

A. DESIGN OF NPSC-IOT

The sucker on the octopus tentacle is composed of two chambers. The outer chamber is an organ like a funnel, and the inner chamber is like a mortar socket of pestle, as shown in Fig.1 [32]. The edge tissue of the octopus is the soft tissue that expands outward, and has a certain radian, which forms an outer air cavity with the contact plane; the throttling orifice is a narrow channel that the edge of the sucker converges to the center and connects the inner and outer gas chambers, and has the switching function. The air cavity and the acetabulum are the muscle tissues that form the inner air cavity, and adjusting the muscle contraction can form negative pressure. The bottom muscle is the muscle tissue that connects the octopus tentacles and the edge of the sucker. The rigidity is stronger than the edge tissue, which can provide the force point for the force of the sucker. When the tentacle of the octopus is to absorb the target object, the bottom muscle will shrink, which will deform the edge tissue so that it can perfectly fit to the target object, thus forming a closed external air cavity. At this time, the air chamber and the acetabulum begin to shrink, causing a strong negative pressure inside the sucker. The tighter the muscle contraction of the socket, the greater the negative pressure, and the stronger the sucker. The larger the sucker, the greater the adsorption force [28]. The octopus sucker has the characteristics of small size and large load capacity. In this paper, NPSC-IOT is designed as the tentacle of inchworm robot to improve its load capacity.

In this paper, NPSC-IOT is designed as shown in Fig.2(a). The structure is mainly composed of sucker adsorption plate, silica gel edge, bleeder hole, vacuum pump, air pressure sensor, solenoid valve, outlet 1, outlet 2, foaming strip, silica gel fixing and module connector. The silica gel edge simulates the edge tissue of the octopus sucker, and the sucker adsorption plate and the contact plane form the outer cavity. The sucker bleeder hole and the solenoid valve connect the channel of the external air chamber and the vacuum pump, and have the switching function. The vacuum pump is used to simulate the ability of the octopus sucker muscle to contract the inner air cavity to form a negative pressure. When the sucker is adsorbed, the sucker adsorption plate and the adsorption plane can be closely fitted. Under the negative pressure control, the adsorption pressure of the sucker can be adjusted to meet the demand of the trunk structure movement for force.

The NPSC-IOT is installed at the end of BSIR as the tentacles of the robot. When the inchworm robot moves, the NPSC-IOT adsorbs support surface to provide support for the BSIR's movement. In order to ensure the stability of the inchworm robot movement, the sucker is required to provide a continuous and stable support force, that is, the sucker is required to provide a stable adsorption pressure. When the volume of the outer air cavity composed of the suction plate and the contact plane is too large, the adsorption pressure is unstable. Therefore, we designed the contact surface of the sucker adsorption plate as a matrix block structure to reduce the volume of the outer air cavity and improve the stability of the adsorption pressure. The contact surface structure of the suction plate is shown in Fig.2 (b). The structure can not only increase the contact area, but also reduce the negative pressure space of the sucker.

The edge of the silicone rubber is the outer sealing structure of the sucker structure. The edge structure is prior to the contact plane of the sucker adsorption plate. In the process of mutual extrusion, the outer space of the edge can form a negative pressure space first to improve the adsorption success rate. Due to the less degree of freedom of the robot 's motion control, in some postures, the sucker structure cannot adsorb the plane from the vertical direction, and must be close to the plane from the side. If the sucker adsorbs the plane at a certain inclination angle, some positions of the sucker in the structure without the edge of the silica gel can't fit the plane and leak, which reduces the success rate of adsorption. The increased silica gel edge structure can form a negative pressure space before the contact plane of the sucker plate to assist the suction of the sucker, so the sucker is allowed to adsorb the target at a certain deviation angle, thereby reducing the control difficulty.

The center of the suction plate is the bleeder hole of the sucker, and a foaming strip with a diameter slightly larger than the groove spacing is inserted into the outer ring of the groove. In the case of extrusion, the foam strip will shrink, making the sucker plate close to the moving plane. At the same time, as the barrier of internal and external air pressure, it is the sealing structure of the inner layer of the sucker. The silica gel fixation is used to fix the silica gel edge structure covered on the sucker adsorption plate, increase the sealing of the silica gel edge structure and the connection stability with the sucker adsorption plate. The module connector is used to connect the sucker module with the rotating shaft of the transverse servo motor to enhance the stability of the sucker module to the robot support. The pressure sensor is used to monitor the pressure inside the sucker, and adjust the output of the vacuum pump according to the output value of the sensor, so as to control the adsorption force of the sucker adsorption plate. The solenoid valve is used to quickly release the negative pressure space in the air path of the sucker, so that the sucker loses its adsorption force and facilitates the robot to perform the next gait. Outlet 1 is used to release the negative pressure space in the air path of the sucker, and outlet 2 is used for the suction output of the vacuum pump. The vacuum pump is used to provide negative pressure for the gas path of the sucker, so that the sucker produces negative pressure, thereby adsorbing the contact plane, and adjusting the output of the vacuum pump can adjust the adsorption force of the sucker.

B. CONTROL MODEL OF SUCKER

The bionic sucker adjusts the adsorption force by controlling the negative pressure of the external air chamber. When the solenoid valve is turned off, the sucker does not provide suction. When the solenoid valve is closed, the sucker provides adsorption force. At this time, the adsorption force is adjusted by controlling the vacuum pump. The control scheme is shown in Fig.3, and the closed-loop control is realized by using the feedback data of the air pressure sensor. For closed-loop control systems, PID control is usually

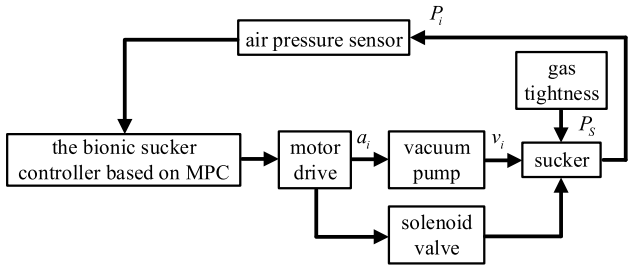

FIGURE 3. Closed-loop control scheme of sucker.

used to meet system requirements. However, the PID control algorithm does not predict the model, and its performance depends on the adjustment of parameters. The MPC control method can overcome this defect, and its control process is based on the model prediction of the current state to the future state, which can quickly adjust the output. MPC control is superior to PID control in response speed and control workload. At present, the MPC control method is widely used in the field of vehicle control, and the control object is the driving motor of the vehicle. The control process of vehicle drive motor is similar to the vacuum pump control in this paper [34], [35], [36]. In this paper, MPC control algorithm is used to adjust the adsorption force of bionic sucker.

The MPC control algorithm adjusts the suction force of the sucker by changing the flow rate of the vacuum pump. The algorithm collects the pressure data of the sucker to predict the future operating state and correct the output expectation of the flow rate variation of the vacuum pump. According to the control process in Fig.3, in this control algorithm, the pressure value P in the sucker and the flow rate v of the vacuum pump are state variables, P_{i-1} and P_i represent the pressure values of the previous moment and the current moment respectively; v_{i-1} and v_i represent the flow rate of the vacuum pump at the previous moment and the current moment, respectively. The flow rate variation is the control quantity. a_{i-1} and a_i represent the flow rate variation of the vacuum pump at the previous moment and the current moment respectively; e_P represents the pressure error in the sucker; e_v represents the flow rate error of the vacuum pump. The sucker model equation based on MPC is established as shown in Equation (1).

$$\begin{cases} e_P = P_{i-1} - P_i - v_i T + P_s \\ e_v = |v_{i-1} - v_i| \\ P_i = P_{i-1} - \dfrac{v_{i-1}T}{V_0} - \dfrac{a_{i-1}T^2}{2V_0} \\ v_i = v_{i-1} + T \end{cases} \tag{1}$$

where V_0 is the space volume inside the sucker; P_s is the air-tight leakage pressure; T is the time constant. The state space equation of the sucker is established as shown in Equation (2).

$$\dot{\boldsymbol{x}}(t) = \boldsymbol{A}\boldsymbol{x}(t) + \boldsymbol{B}_u\boldsymbol{u}(t) + \boldsymbol{B}_\lambda \lambda(k) \tag{2}$$

where $\boldsymbol{x}(t) = [e_P, e_v, P_i, v_i]$ is the system state quantity; $\boldsymbol{u}(t) = a_i$ is the system control quantity; $\lambda(k)$ is the system

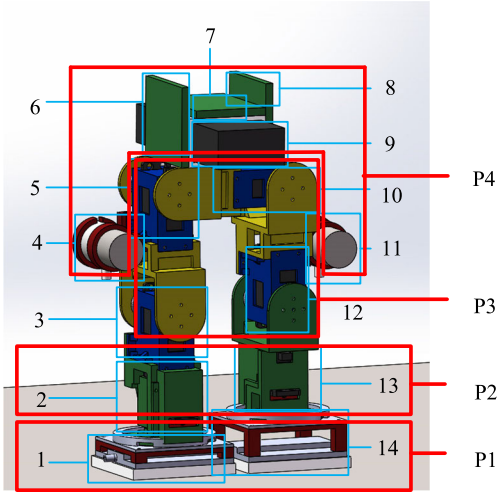

FIGURE 4. The overall mechanical structure of the robot.

TABLE 1. The name of each module of the robot marked in Fig.4.

label	Robot module name
1	Back-end sucker structure
2	Back-end transverse servo motor
3	Longitudinal servo motor 1
4	back-end sucker vacuum pump
5	Longitudinal servo motor 2
6	Extended circuit board
7	System control board
8	Motor drive board
9	Battery
10	Longitudinal servo motor 3
11	Front-end sucker vacuum pump
12	Longitudinal servo motor 4
13	Front-end transverse servo motor
14	Front-end sucker

TABLE 2. Parameters of TD-8120 motor.

Parameter	Parameter value
Weight	65g
Motor Size	40*20.5*40.5mm
Working Voltage	5V~8.4V
Locked-Rotor Current	2.1A~2.7A
Driving Method	PWM
Pulse Width Range	200-2500us
Rotation Range	-90° ~ 90°

measurement error; $\boldsymbol{A}$, $\boldsymbol{B}_u$ and $\boldsymbol{B}_\lambda$ are the state coefficient matrix, the input control coefficient matrix and the measurement interference coefficient matrix, which can be obtained by solving the Jacobian matrix by the Taylor expansion of Equation (5).

C. DESIGN OF BIONIC SUCKER CONTROLLER BASED ON MPC

In the above established state space equation, two objective functions including response speed and accuracy based on the principle of MPC algorithm are introduced. Assuming the

TABLE 3. Overall specification parameters of the robot.

Parameter	Parameter value
Weight	1.54kg
Payload	500g
Maximum speed of servo motor	0.1s/60°
DOF	6
Extended length	430mm
Accuracy	±5mm
Range of motion	170mm

sampling period T, the discrete state equation can be obtained according to equation (2) as shown in equation (3).

$$\begin{cases} \dot{\boldsymbol{x}}(k+1) = \boldsymbol{A}_k \boldsymbol{x}(k) + \boldsymbol{B}_k \boldsymbol{u}(k) + \boldsymbol{B}_{\lambda k} \lambda(k) \\ \boldsymbol{y}(k) = \boldsymbol{C}_k \boldsymbol{x}(k) \end{cases} \tag{3}$$

where $\boldsymbol{A}_k = \boldsymbol{I} + \boldsymbol{A}T$, $\boldsymbol{I}$ is the unit matrix; $\boldsymbol{B}_k = \boldsymbol{B}_u T$; $\boldsymbol{B}_{\lambda k} = \boldsymbol{B}_\lambda T$; $\boldsymbol{C}_k = diag(1, 1, 1, 1)$. The control input $\boldsymbol{u}$ is replaced by the control increment $\boldsymbol{\Delta u}$. The control process is realized by controlling the flow rate variation of the vacuum pump $\boldsymbol{a_i}$. The relationship between the control increment $\Delta \boldsymbol{u}$ and the control input $\boldsymbol{u}$ is shown in Equation (4).

$$\boldsymbol{u}(k+j|k) = \boldsymbol{u}(k+j-1|k) + \Delta \boldsymbol{u}(k+j|k) \tag{4}$$

The model prediction state equation is shown in Equation (5).

$$\boldsymbol{Y}(k) = \boldsymbol{D}\boldsymbol{x}(k) + \boldsymbol{F}\Delta \boldsymbol{U}(k) + \boldsymbol{G}\boldsymbol{u}(k-1) + \boldsymbol{H}\lambda(k) \tag{5}$$

where $\boldsymbol{Y}(k)$ is the predictive output of the control part at time k for the future time domain $\boldsymbol{N_P}$, $\boldsymbol{N_P}$ is set to 30; $\boldsymbol{\Delta U}(\boldsymbol{k})$ is the sum of control increments in the control time domain. $\lambda(\boldsymbol{k})$ is the error interference in the model at time k, which is the air tightness effect of the sucker structure in this paper. $\boldsymbol{D}$, $\boldsymbol{F}$, $\boldsymbol{G}$, $\boldsymbol{H}$ are coefficient matrices. Through the current state variable $\boldsymbol{x}(k)$ and the control increment $\boldsymbol{\Delta U}$, the future state variables and output variables of the system can be predicted. The objective function with relaxation factor is established as shown in Equation (6).

$$\boldsymbol{J}_k = \sum_{j=1}^{N_P} ||y(k+j|k) - y_r(k+j|k)||_Q^2 + \sum_{j=0}^{N_c} ||\boldsymbol{\Delta u}(k+j|k)||_R^2 + \rho\varepsilon^2 \tag{6}$$

where $\boldsymbol{N_c}$ is the control time domain, set to 5; $y(k+j|k)$ and $y_r(k+j|k)$ are the current pressure value and the expected pressure value respectively; $\boldsymbol{Q}$ and $\boldsymbol{R}$ are the coefficient matrix of self-control target. In this paper, the error weight coefficient $\boldsymbol{Q} = 5\boldsymbol{I}$, the ride comfort weight coefficient $\boldsymbol{R} = 5\boldsymbol{I}$, $\boldsymbol{R}$ is the unit matrix. The relaxation factor is added to the objective function, which is used to represent the range of system fluctuation. At the same time, in order to avoid the system having no solution in the solution, ε is the relaxation factor of the system. ρ is the weight coefficient of the parameter. The deviation of the system is shown in Equation (7).

$$\boldsymbol{E}(k) = \boldsymbol{Y}_r(k) - \boldsymbol{W}_r \boldsymbol{x}(k) - \boldsymbol{W}_u \boldsymbol{u}(k-1) + \boldsymbol{W}_\lambda \lambda(k) \tag{7}$$

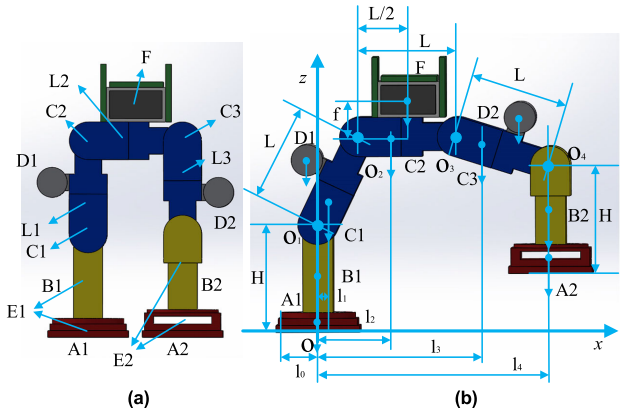

FIGURE 5. Robot motion posture: (a) Initial attitude (b) General attitude.

where $\boldsymbol{W}_x$, $\boldsymbol{W}_u$ and $\boldsymbol{W}_\lambda$ are coefficient matrices. Through equation (6) and equation (7), the standard quadratic programming function can be obtained as shown in Equation (8).

$$\min_{\Delta \boldsymbol{U}} \left(\frac{1}{2} \Delta \boldsymbol{U}^T \boldsymbol{Z} \Delta \boldsymbol{U} + \boldsymbol{f}^T \Delta \boldsymbol{u} \right) \tag{8}$$

$$\begin{cases} \boldsymbol{Z} = \begin{bmatrix} 2\boldsymbol{W}_{\Delta u}^T \boldsymbol{Q} \boldsymbol{W}_{\Delta u} & 0 \\ 0 & \rho \end{bmatrix} \\ \boldsymbol{f} = -2\boldsymbol{W}_{\Delta u}^T \boldsymbol{Q} \boldsymbol{E}(k) \end{cases} \tag{9}$$

where $\boldsymbol{W}_{\Delta u}$ is the left multiplication $\boldsymbol{C}_k$ of the block matrix in the parameter matrix $\boldsymbol{F}$. The constraints of state variable, input control variable and input control increment are shown in Equation (10).

$$\begin{cases} \boldsymbol{u}_{min} + \varepsilon \boldsymbol{v}_{min} \le \boldsymbol{u}(k+j|k) \le \boldsymbol{u}_{max} + \varepsilon \boldsymbol{v}_{max} \\ \Delta \boldsymbol{u}_{min} + \varepsilon \boldsymbol{v}_{min} \le \boldsymbol{u}(k+j|k) \le \Delta \boldsymbol{u}_{max} + \varepsilon \boldsymbol{v}_{max} \\ \boldsymbol{y}_{min} + \varepsilon \boldsymbol{v}_{min} \le \boldsymbol{y}(k+j|k) \le \boldsymbol{y}_{max} + \varepsilon \boldsymbol{v}_{max} \end{cases} \tag{10}$$

where $\boldsymbol{u}_{min}$ and $\boldsymbol{u}_{max}$ are the minimum and maximum values of the input control quantity respectively; $\Delta \boldsymbol{u}_{min}$ and $\Delta \boldsymbol{u}_{max}$ are the minimum and maximum values of control increment, respectively. $\boldsymbol{y}_{min}$ and $\boldsymbol{y}_{max}$ are the minimum and maximum values of the system output respectively. $\varepsilon \boldsymbol{v}$ is the relaxation range of the upper and lower boundaries; $\boldsymbol{v}$ is the current flow rate of the vacuum pump.

According to Equation (14), the expected flow rate variation of the vacuum pump at time k can be solved, and the expected speed at time k is obtained as shown in Equation (11).

$$\boldsymbol{v}(k) = \boldsymbol{u}(k) = \boldsymbol{u}(k-1) + \Delta \boldsymbol{u}(k) \tag{11}$$

$\boldsymbol{u}(k)$ is the next input control quantity feedback to the system loop, forming a closed-loop control.

III. THE MOTION ANALYSIS OF INCHWORM ROBOT BASED ON MPC-BSC

A. BIONIC SUCKER INCHWORM ROBOT STRUCTURE

In this paper, BSIR is developed, and its overall structure is shown in Fig. 4. The robot mainly includes four parts: sucker, transverse servo motor group, longitudinal servo motor group and other components. The sucker is the P1 part in Fig.4, which is installed at the tentacle position at both ends of the inchworm robot to realize the foot function under the torso when the inchworm is moving. The transverse servo motor group and the longitudinal servo motor group cooperate to realize the trunk function of the robot. The transverse servo motor structure is the P2 part in Fig.4, which provides the steering function for the robot motion. The longitudinal servo motor unit is the P3 part in Fig.4, which provides the robot with the function of stretching and shrinking to produce displacement difference, and mainly controls the alternating adsorption of suckers. The other parts are the P4 part in Fig.4, including the battery and the drive control circuit of the robot. The quality of these parts cannot be ignored during the movement of the robot. Table 1 shows the robot parts represented by the label in Fig.4. The driver of BSIR adopts a TD-8120MG servo motor. The motor parameters are shown in the Table 2. Based on the mechanical structure of the robot, the motion range of the robot can be obtained. The overall specification parameters of the robot are shown in Table 3.

TABLE 4. Robot parameter table.

Symbol	Explanation
A1	Back-end sucker structure
A2	Front-end sucker structure
B1	Back-end transverse servo motor
B2	Front-end transverse servo motor
C1	Longitudinal servo motor 1
C2	Longitudinal servo motor 2
C3	Longitudinal servo motor 3
D1、D2	Vacuum pump
L1	Trunk joint 1 (combination of C1 and D1)
L2	Trunk joint 2
L3	Trunk joint 3 (combination of C3 and D2)
F	Battery
E1	The combination of A1 and B1
E2	The combination of A2 and B2
O	The central point of A1
O_1	Shaft of the longitudinal servo motor 1
O_2	Shaft of the longitudinal servo motor 2
O_3	Shaft of the longitudinal servo motor 3
O_4	Shaft of the longitudinal servo motor 4
L	Length of trunk joints 1, 2, 3
H	The length of combination E1 or E2
l_0	Arm length of sucker
l_1	The distance from the centroid of L1 to O
l_2	The distance from the centroid of L2 to O
l_3	The distance from the centroid of L3 to O
l_4	The distance from the centroid of E2 to O
f	The distance from F centroid to joint L2
m_0	The mass of A1 is 80 g
m_1	The mass of A2 is 164 g
m_2	The mass of B1 or B2 is 78 g
m_3	The mass of C1 or C2 or C3 is 62 g
m_4	The mass of D1 or D2 is 62 g
m_5	The mass of F is 442 g

B. ANALYSIS OF SUCTION CUP FORCE

The adsorption force provided by the sucker is related to the contact area and pressure of the sucker. The contact

part between the sucker and the target object includes the silica gel edge and the sucker adsorption plate. The silica gel edge function is to provide the sealing function of the external gas chamber. The sucker adsorption plate provides a contact surface with the object. The pressure is provided by the vacuum pump. The pressure provided by the vacuum pump can be controlled by programming. Therefore, in order to ensure the stable movement of the inchworm robot, it is necessary to determine the size of the suction plate. First of all, we need to determine the maximum torque applied by the robot to the force point, and clarify the minimum adsorption force required by the sucker. Then, the mathematical model between the size of the suction plate and the adsorption force is established.

The torque of the robot during the movement is constantly changing. We analyze the torque of each part of the structure on the sucker during the movement of the robot.

The motion posture of the robot is shown in Fig.5, and the parameters of each part of the robot are shown in Table 4. Because the mass of the longitudinal servo motor C1, C2, C3, the vacuum pump D1, D2 and the longitudinal servo motor is consistent, the centroid of the servo motor C1 and the centroid of the vacuum pump D1 can be regarded as the whole of the joint L1, and the centroid is at the midpoint of the L1. The servo motor C3 and the vacuum pump D2 can be regarded as the whole of the joint L3, and the centroid is at the midpoint of the L3. Similarly, the sucker structure A2 and the steering structure B2 are also regarded as a straight rod E2 with a center of mass at the midpoint. Due to the large mass of the battery, it is not suitable for simplification and needs to be considered separately.

According to the general posture shown in Fig.5 (b). The torques I_1, I_2, I_3, I_4 and I_5 exerted by joint L1, joint L2, joint L3, sucker structure and steering structure E2 and battery F on sucker structure A1 are shown in Equation (12). The total torque I applied by the robot to the sucker structure A1 is shown in Equation (13).

$$\begin{cases} I_1 = (m_3 + m_4)\, g \left(\frac{L}{2} \sin\theta_1\right) \\ I_2 = m_3 g \left(L\, sin\theta_1 + \frac{L}{2} cos\,(\theta_2 - \theta_1)\right) \\ I_3 = (m_3 + m_4)\, g \\ \left(L\, sin\theta_1 + \frac{L}{2} cos\,(\theta_2 - \theta_1) + \frac{L}{2} sin\theta_4\right) \\ I_4 = (m_0 + m_2)\, g \\ \left(L\, sin\theta_1 + \frac{L}{2} cos\,(\theta_2 - \theta_1) + L\, sin\theta_4\right) \\ I_4 = (m_0 + m_2)\, g \\ \left(L\, sin\theta_1 + \frac{L}{2} cos\,(\theta_2 - \theta_1) + L\, sin\theta_4\right) \end{cases} \tag{12}$$

$$I = I_1 + I_2 + I_3 + I_4 + I_5 \tag{13}$$

The torque exerted by the robot 's motion attitude on the sucker structure A1 and the adsorption force F_S provided by the sucker are shown in Equation (14).

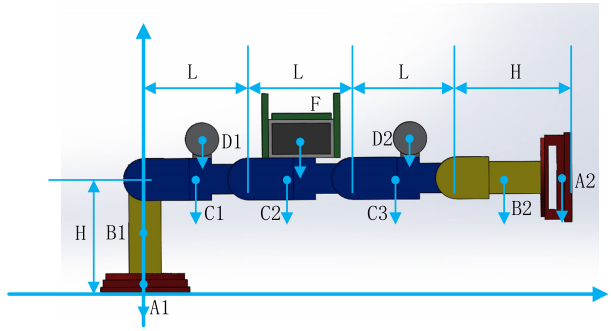

FIGURE 6. The theoretical attitude of the maximum adsorption force required by the robot.

TABLE 5. Vacuum pump parameter table.

Voltage range	5V-8.4V
Operating current	1A
Working maximum negative pressure	50kPa
Weight	62g
Work Flow	1L/min（5V）

$$F_S = \frac{I_1 + I_2 + I_3 + I_4 + I_5}{l_0} \tag{14}$$

When $\theta_1 = \theta_2 = \theta_3 = \frac{\pi}{2}$, $\theta_4 = 0$, the robot 's posture is shown in Fig.6. At this time, the robot 's parts exert the maximum torque $I_{max} = 15.9\ kg \cdot cm$ on A1. According to the equation (14), the minimum adsorption force F_S required by the sucker at this time can be obtained to be about 65.0 N.

The vacuum pump parameters selected in this paper are shown in Table 5, and the negative pressure value provided by the air pump can be controlled by programming. According to the equation (15), the area S of the sucker adsorption plate can be calculated.

$$F_S = PS \tag{15}$$

When $F_S = 65.0N$, $S = 20.3cm^2$. When the area of the suction plate is greater than $20.3cm^2$, it can provide a stable adsorption force for the movement of the robot. In the design process of the sucker, we added redundancy, and set the size of the gas chamber of the sucker adsorption plate to 48mm * 48mm, and the edge size of the silica gel to 68mm * 68mm. Considering providing a suitable arm l_0 for the adsorption force of the sucker, we design the sucker adsorption plate as a square. We use 3D printing technology (hot melt remodeling printing technology) to print the sucker plate. The material is ABS (a terpolymer of acrylonitrile, 1,3-butadiene and styrene monomers). The physical diagram of the sucker structure is shown in Fig.7.

C. MOTION ANALYSIS BASED ON MPC-BSC

In this paper, the bionic sucker controller based on MPC is used to control BSIR to realize the 'Ω' motion gait. Fig.8 is the simplified diagram of the robot, which is convenient for

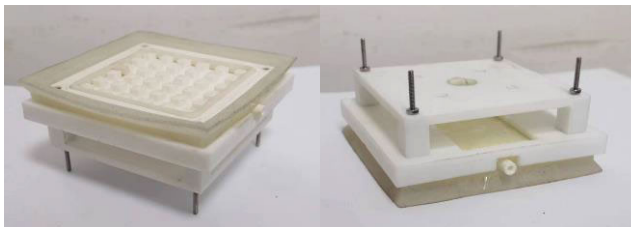

FIGURE 7. The physical drawing of sucker structure.

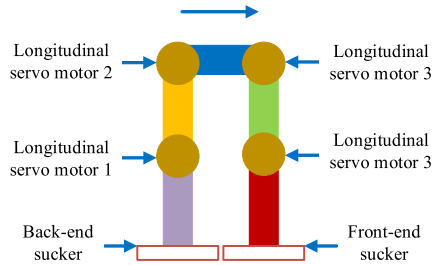

FIGURE 8. Simplification of robot.

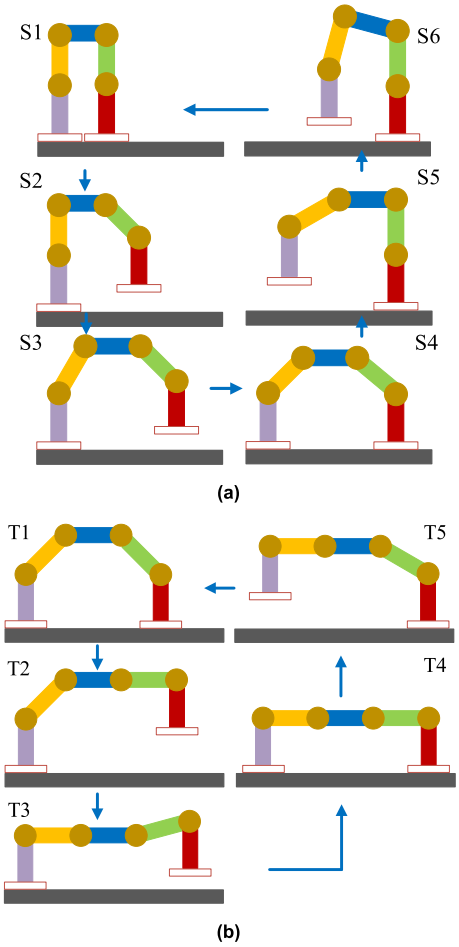

FIGURE 9. Two postures of the robot moving in the horizontal plane.

understanding the position of each part of the robot during the movement. In order to better explain the movement process of the robot, we assume that when the robot moves in the horizontal plane, the direction of the robot is from left to right. Fig.9 describes the movement gait of the BSIR in the horizontal plane. Through the contraction and extension of the trunk structure, the sucker is moved, so that the front-end and back-end suckers alternately adsorb attachments to achieve walking function. In order to test the performance of the bionic sucker, we designed two gaits as shown in Fig.9. The first gait is shown in Fig.9 (a). Firstly, the robot is in the initial state, that is, the trunk structure shrinks, and the minimum distance between the front-end and back-end suckers is the S1 attitude in Fig.9 (a). Then the back-end sucker adsorbs the plane and reaches a stable state of adsorption. The front-end sucker is lifted, and the front-end longitudinal servo motor extends to move the front-end sucker forward, which is the S2 attitude in Fig.9 (b). Next, the back-end longitudinal servo motor controls the front-end and back-end suckers to expand by adjusting the rotation angle, and the front-end sucker is ready for adsorption, which is the S3 attitude in Fig.9 (a). The front-end sucker falls down and begins to adsorb the plane and reaches a stable state of adsorption. The electromagnetic valve of the back-end sucker disconnects the gas path and releases the negative pressure to make the back-end sucker suspended, which is the S4 attitude in Fig.9 (a). The front-end longitudinal servo motor shrinks and the back-end sucker is lifted, which is the S5 attitude in Fig.9 (a). Finally, the back-end longitudinal servo motor shrinks and moves the back-end sucker to the front-end sucker near the plane to prepare the adsorption plane, which is the S6 attitude in Fig.9 (a). The back-end longitudinal servo motor continues to shrink until the back-end sucker is close to the plane and adsorbed. When the back-end sucker reaches a stable state of adsorption, it returns to the S1 attitude and completes a step motion. In the normal forward motion, during the transition from S6 attitude to S1 attitude in Fig.9 (a), the sucker at the front-end can directly perform S2 attitude without adsorbing the plane, reducing the running time of attitude transition.

The second gait is shown in Fig.9 (b), which is a kind of gait derived from the height adjustment of the first gait according to the current environmental situation. Firstly, the robot is limited to a high impact and in a shrinking state, which is the T1 attitude in Fig.9 (b). Then the back-end sucker adsorbs the plane and reaches a stable state of adsorption. The front-end sucker is lifted, and the front-end longitudinal servo motor extends to move the front-end sucker forward, which is the T2 attitude in Fig.9 (b). Next, the back-end longitudinal servo motor controls the front-end and back-end suckers to expand by adjusting the rotation angle, and the front-end sucker is ready to adsorb. Different from the first posture, the trunk structure will stretch to the maximum length, which is the T3 posture in Fig.9 (b). The front-end sucker falls down and begins to adsorb the plane and reaches a stable state of adsorption. The electromagnetic valve of the back-end sucker disconnects the gas path and releases the negative pressure to make the back-end sucker suspended, which is the T4 attitude

in Fig.9 (b). The front-end longitudinal servo motor shrinks and the back-end sucker is lifted, which is the T5 attitude in Fig.9 (b). Finally, the back-end longitudinal servo motor shrinks the trunk structure. After reaching the height limit, the back-end sucker is close to the plane and adsorbed, that is, returning to the T1 posture in Fig.9 (b) to complete a step action. Due to the extension of the torso part is too long, the tension applied to the sucker in the adsorption state is large, and it is not recommended to turn the movement. Therefore, in the case of height limitation, only a certain distance can be contracted to set aside displacement margin for the next extension.

Based on our designed robot gait plan, we can design the control process of the robot during movement, and provide more detailed control to the robot to complete the motion gait. In the pose planning of biomimetic inchworm robots, the choice between different poses is determined by two conditions: the stride length of the robot completing the stride gait and the maximum point that the robot is limited to reach during the motion process. The motion attitude of the robot is controlled according to the motion environment, motion requirements and other conditions. The attitude control process we designed is shown in Fig.10. Firstly, the pose limit that the robot can reach and the step size range for step motion are determined based on the limitations of the motion environment, in order to determine the initial state of the robot, as shown in Fig.9 for two different heights of poses; Select the appropriate step size within the robot's step range, calculate the step attitude using the principle of forward and inverse kinematics of the robot, and determine the rotation angle of each servo motor in the step attitude, as shown in S2 and S3 in Fig.9 (a) and T2 and T3 in Fig.9 (b); According to the force analysis process of robot motion posture proposed by us, the minimum adsorption force that the suction cup should provide can be calculated under the corresponding robot posture. We control the suction cup adsorption force to 1.2 times the minimum value, thereby reducing the power consumption of the vacuum pump; By determining the step size and transition posture, we ultimately obtain the robot's switching posture, which facilitates the switching of suction cup structure for adsorption and release, as shown in the S4 posture in Fig.9 (a) and the T4 posture in Fig.9 (b); After completing the posture switch, the robot's transition posture is still limited by height, and then the posture corresponding to the first half stage transitions to the initial posture, completing a step motion.

The forward motion of the robot is a cyclic process of step motion, and the step size of the step motion is controllable. The backward motion of the robot is an inverse cycle process of step motion.

The bionic sucker designed in this paper expands the movable environment of the inchworm robot, so that the robot can move on both horizontal and vertical planes with different inclination angles. Fig.11 shows the motion process of the robot in the vertical plane. During the operation of the robot, the adsorption force on the sucker is calculated in real time

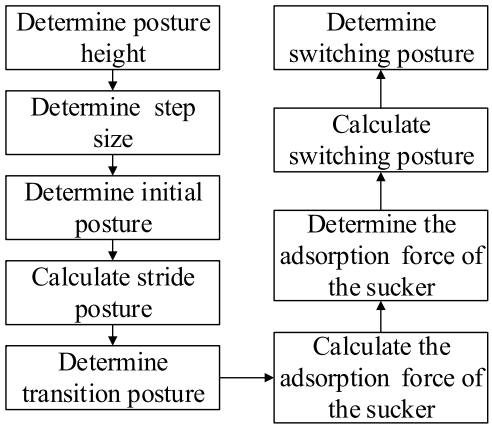

FIGURE 10. Control process of posture change.

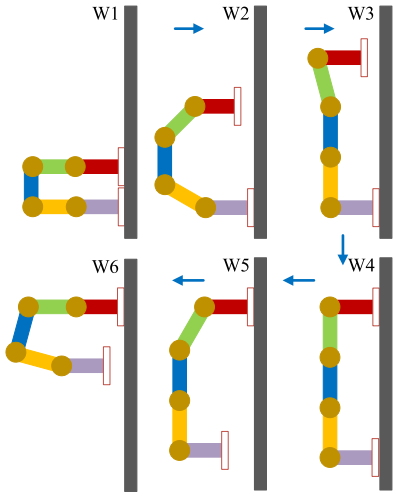

FIGURE 11. Motion process of robot in vertical plane.

according to equation (14). The bionic sucker controller of MPC adjusts the negative pressure of the vacuum pump to provide the adsorption force and ensure the stable movement of the robot.

D. STEERING MOTION ANALYSIS

Since the inchworm robot adds a transverse servo motor unit, the robot can achieve a steering gait. The inchworm robot has certain requirements for the space size to complete the steering gait. Next, we calculate the minimum space required for the inchworm robot to complete the steering.

In order to show the steering motion process of the inchworm robot, we use the robot 's top view to describe the process. Based on the overall structure of the robot in Fig.4, the top view of the robot can be obtained as shown in Fig.12. When the robot is in the initial attitude S1, the steering process of the robot is shown in Fig.13. The inchworm robot turns the initial state as shown in the X1 pose in Fig.13, and there is a certain distance between the two suckers d_0; when the robot performs a large-angle steering motion, the torso part will appropriately increase the step length of the step according to the steering angle to ensure that the two

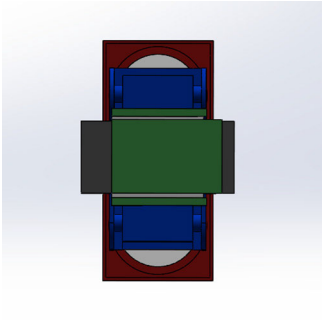

FIGURE 12. Top view of robot in initial pose.

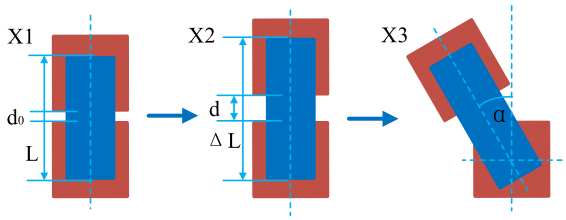

FIGURE 13. The simplified view of the robot during the steering process.

suckers will not collide with each other during the steering process. As shown in Fig.13, the distance between the two suckers after the robot increases the step length d; after completing the step motion, the robot performs a steering motion, as shown in the X3 pose in Fig.13, α is the angle of the robot 's steering.

During the above steering process, the distance d between the two suckers plays a crucial role in adjusting the steering angle. d_0 is the initial value of the distance between two suckers, which is determined by the mechanical structure. When the robot performs a small angle steering motion, d_0 can meet the displacement difference caused by the sucker steering, so it does not need to perform step motion. When steering at a large angle, the distance between the two suckers needs to be increased to meet the displacement difference required for steering.

According to the attitude process of the robot steering, we derive the relationship between the steering angle and the distance between the two suckers as shown in Equation (16).

$$\begin{cases} D = D_1 + D_1 \tan\alpha + \dfrac{D_1}{\cos\alpha} \\ d = D_1 \sin\alpha \\ d = \dfrac{D \sin\alpha \cos\alpha}{1 + \sin\alpha + \cos\alpha} \end{cases} \tag{16}$$

The D_1 in the equation (16) is the distance from the intersection point to the edge of the sucker, which is generated by the intersection of the position of the sucker on the steering center axis after steering and the position before steering in Fig.12, as shown in Fig.14. D is the side length of the sucker. From Equation (16), it can be obtained that the spacing d of the two suckers changes with the rotation angle α. Under the condition that the distance between the two suckers d is the initial distance d_0 and there is no collision during the steering process, the maximum steering angle of the steering motion can be obtained to be about 32°. When the steering angle exceeds 32°, the distance d between the two suckers will exceed the initial distance. The robot needs to increase the step size to adapt to the displacement difference caused by the steering motion, so as to ensure that the two suckers do not collide. The required step size is increased by rotating the θ_1 angle through the longitudinal servo motor 1, as shown in Equation (17).

$$\theta_1 = \sin^{-1}\left(\frac{d - d_0}{L}\right) \tag{17}$$

It can be obtained from Eq. (16) that when the rotation angle $\alpha = 45°$, the distance d between the two suckers is 15.3 mm, which is the maximum distance between the two suckers. The maximum circular space radius r_0 required for the robot steering process is shown in equation (18).

$$r_0 = \sqrt{\left(\frac{3}{2}D + d\right)^2 + \left(\frac{1}{2}D\right)^2} \tag{18}$$

The radius r_0 of the maximum circular space can be calculated to be 131.6 mm by Equation (18). In this range, the robot can ensure free steering without collision.

IV. EXPERIMENTAL TEST

A. SUCKER TEST

In order to test the adsorption force of the sucker on different material planes, we built a sucker adsorption force test platform as shown in Fig.15. Experimental conditions: vacuum pump power supply voltage constant 5V; the test equipment is Edberg push-pull meter; the test planes are metal plane, wood plane, glass plane, ceramic tile plane and wall plane respectively. The roughness of the metal plane is about Ra0.8, the roughness of the wooden plane is about Ra200, the roughness of the glass plane is about Ra0.006, the roughness of the ceramic tile plane is about Ra0.1, and the roughness of the wall surface is about Ra1000. The pull direction is perpendicular to the adsorption plane.

We define a test experiment process as the tension applied to the sucker increases from 0 to the sucker deforms or falls off from the adsorption plane. The tension value was recorded in each experiment. Ten test experiments were carried out on different material planes, and the test results are shown in Fig.16. The 10 tests of the sucker on the above five different material planes all ended when the sucker deformed, and no sucker fell off.

In order to verify the importance of the silicone edge of the cup, we tested the adsorption force of the cup without silicone edge. The experimental conditions are consistent with the sucker test experiment with silicone edge, and the test results are shown in Fig.17. The minimum, maximum, average and variance of the adsorption force test results of the suckers with or without silicone edge on different material planes are

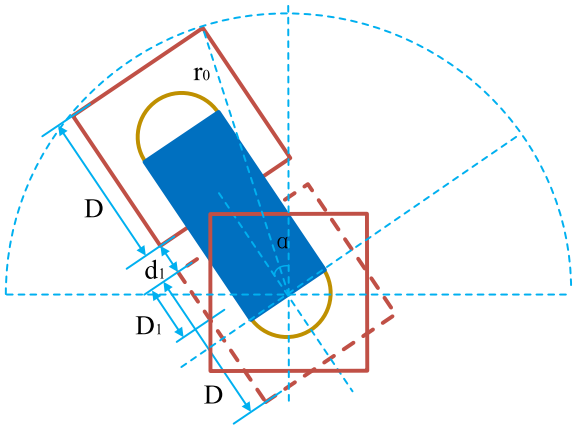

FIGURE 14. Relationship between sucker spacing and rotation angle.

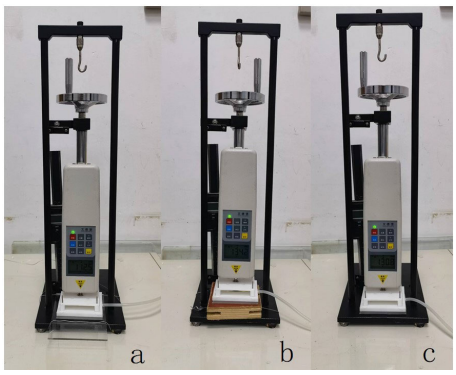

FIGURE 15. Adsorption force test platform of suckers on different material planes.

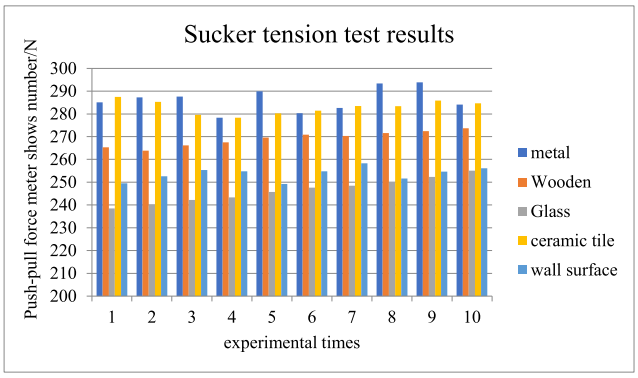

FIGURE 16. Adsorption force test results of suckers with silica gel edges on different material planes.

compared as shown in Table 6 and Table 7. The test results show that the minimum adsorption force of the cup with silica gel edge is much larger than the maximum adsorption force of the cup without silica gel edge. In the sucker test experiment without silica gel edge, the suckers fell off in 10 tests of adsorbing different material planes. The adsorption force of the sucker with the edge of the silicone rubber is much larger than the adsorption force required for the robot to move. The measurement error of the push-pull force meter we selected is ± 0.1N. By correcting the testing platform, we can obtain

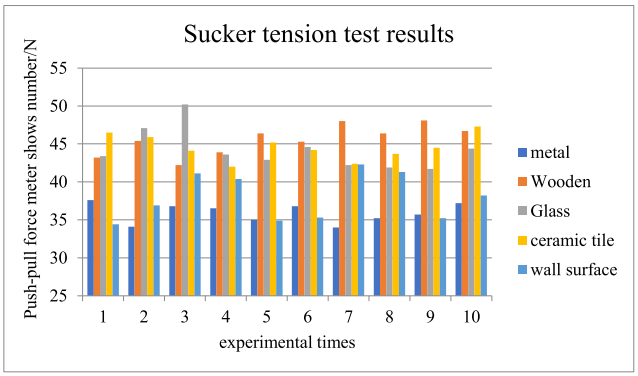

FIGURE 17. Adsorption force test results of suckers without silica gel edges on different material planes.

TABLE 6. Statistical analysis of adsorption force data of suckers with silicone edges on different material planes.

Plane material	Sucker adsorption force			
	minimum	maximum	mean value	variance
Metal plane	278.3N	293.8N	286.23N	26.89
Wooden plane	263.9N	273.7N	269.14N	10.63
Glass plane	238.5N	255.1N	246.34N	28.87
Ceramic tile plane	278.3N	287.5N	282.98N	9.03
wall surface	249.2N	258.3N	253.68N	8.47

TABLE 7. Statistical analysis of adsorption force data of suckers without silicone edges on different material planes.

Plane material	Sucker adsorption force			
	minimum	maximum	mean value	variance
Metal plane	34N	37.6N	35.89N	1.64
Wooden plane	42.2N	48.1N	45.56N	3.87
Glass plane	41.7N	54.2N	44.6N	13.92
Ceramic tile plane	42.0N	47.3N	44.58N	2.864
wall surface	34.4N	42.3N	38N	9.3

that the mechanical error of the platform is within the range of ± 0.5N, so the measurement error for this test is within the range of ± 0.5N.

B. SIMULATION EXPERIMENTS MEASURING THE ADSORPTION FORCE REQUIRED FOR INCHWORM ROBOT MOTION

In order to test the adsorption force required by the inchworm robot during motion, we built an inchworm robot motion force test platform as shown in Fig.18. The test platform is to install the adapter plate at the position of the robot 's sucker A1. A metal wire is drawn at the center point of the adapter plate near the outer 24 mm and connected to the measuring column of the Edberg push-pull meter to keep the metal wire perpendicular to the motion plane. In the motion posture of the robot, two postures are selected as shown in Fig.18 for testing, of which posture 1 is the posture

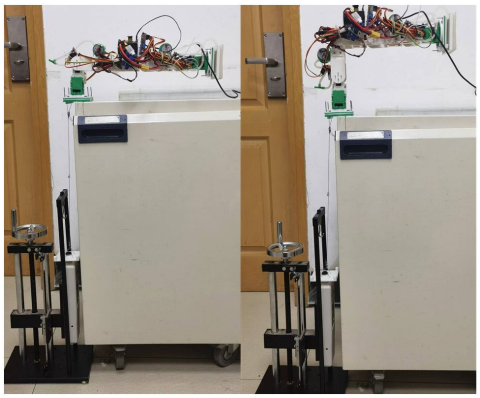

(a) robot posture 1 (b) robot posture 2

FIGURE 18. Sucker force test platform under two postures.

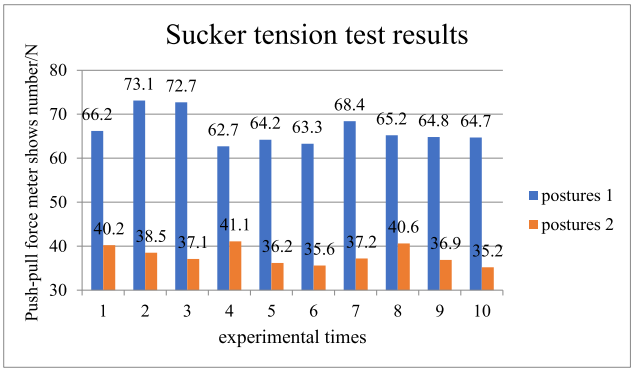

FIGURE 19. Test results of suction cup force in two different postures.

TABLE 8. Test data statistics for two postures.

posture	Tensile force value of the suction cup			
	minimum	maximum	mean value	variance
Posture 1	62.7N	73.1N	66.53N	13.72
Posture 2	35.2N	41.1N	37.86N	4.11

demonstrated above; pose 2 is an arbitrary general pose. During the experiment, the tension at the push-pull gauge is applied to keep the robot stable as shown in Fig.18. When the arm is parallel to the motion plane, the tension value of the push-pull gauge is recorded and repeated 10 times. The test results are shown in Fig.19, the test data statistics for two postures are shown in Table 8. The maximum tensile force measured based on attitude 1 is about 73.1N, the theoretical calculation value is about 65.0N, the maximum measurement error is 12.5%, and the average measurement error is 2.4%; The average tensile force measured based on attitude 2 is 41.1N, the theoretical calculation value is 37.3N, the maximum measurement error is 10.2%, and the average measurement error is 1.5%. Due to the quality of other small parts of the robot and the error factors in the testing process, most of the test results will be larger than the theoretical calculation results.

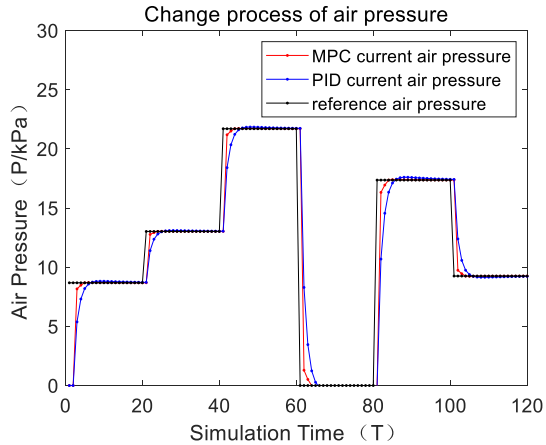

FIGURE 20. Simulation results of suction cup pressure controlled by MPC and PID during robot motion.

C. MPC-BSC TEST

In order to verify the effectiveness of the MPC-based sucker controller, we use MATLAB to simulate and analyze the MPC-based bionic sucker controller. The initial pressure in the sucker is set to 0; the maximum flow rate v of the vacuum pump is $100mL/s$. Signal change period $T = 0.1ms$; the maximum negative pressure P that can be reached in the sucker is $60kPa$. The maximum flow rate variation a of the vacuum pump is $100mL/s^2$. According to the robot motion posture and the robot motion posture torque calculation method shown in Fig.9 (a), the adsorption force that the sucker should provide in the six postures can be obtained, so as to obtain the negative pressure value that the vacuum pump should provide. The simulation results are shown in Fig.20. It can be seen from the simulation results that the negative pressure in the sucker can be quickly reached and stabilized at the reference negative pressure value under the control of the MPC sucker controller. By comparing the negative pressure changes in the sucker controlled by PID, we can see that the pressure in the sucker controlled by MPC can reach the reference negative pressure value faster, showing the rapid response characteristics of MPC control.

We will transplant the MPC based suction cup control algorithm to the bionic inchworm robot control system, adjust the suction force of the suction cup based on the gait selected during the simulation process, and collect pressure data from the pressure sensor, as shown in Figure 21. Due to the fundamental error of the sensor, the initial value is 0.74kPa, and subsequent data increases or decreases above the initial value. The reference values of the control air pressure values corresponding to each posture are marked with dashed lines in the figure. The blue line represents the output result of the suction cup air pressure controlled by PID, and the red line represents the suction cup air pressure data controlled by MPC. We can see from the graph that there is an overshoot in the pressure change of the suction cup controlled by PID, and the response speed is not as fast as the suction cup pressure

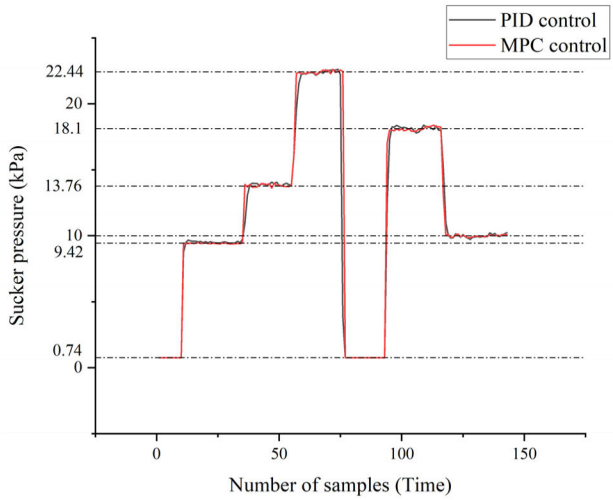

FIGURE 21. Experimental test results of suction cup pressure controlled by MPC and PID during robot movement.

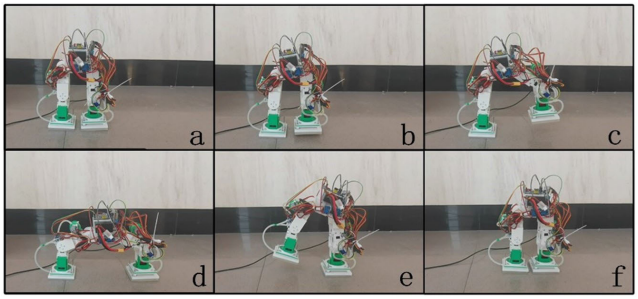

FIGURE 22. Motion process of robot in horizontal tile plane.

controlled by MPC. However, after the pressure stabilizes, the stability of the two control methods is consistent, and the error between the pressure data and the reference value is within $\pm$ 0.2kPa.

D. MPC-BSC INCHWORM ROBOT MOTION TEST

In order to verify the feasibility of the MPC-based bionic sucker controller to control the movement of the inchworm robot on different angle planes, we selected two extreme conditions $\alpha = 0°$ and $\alpha = 90°$ to test the feasibility of the inchworm robot movement. We tested the crawling motion of the robot on the marble tile plane at both horizontal and vertical angles. The test results are shown in Figure 22 and Fig.23. The test results show that the robot can complete the 'Ω' motion gait under different tilt angles. You can see the process of the robot moving on the tile plane at two angles in the videos of Supplementary Materials 1 and 2.

The added bionic sucker can make the inchworm robot move on the plane of different materials. In order to verify this performance, we tested the motion feasibility of the inchworm robot on the vertical tile plane, glass plane and rougher wall, as shown in Fig.24 and Fig.25. The test results show that the robot can complete the 'Ω' motion gait in different material planes. You can see the process of the robot

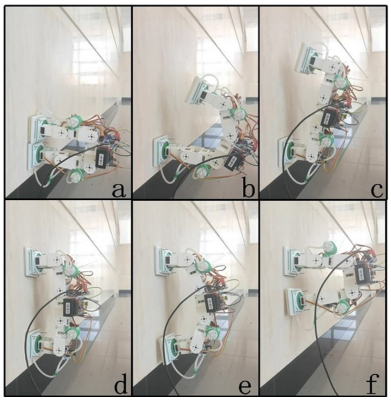

FIGURE 23. Motion process of robot in vertical tile plane.

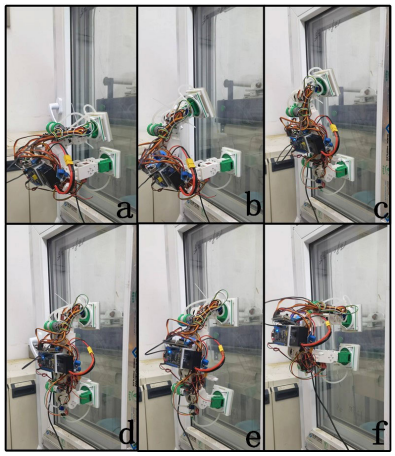

FIGURE 24. Motion process of robot on vertical glass surface.

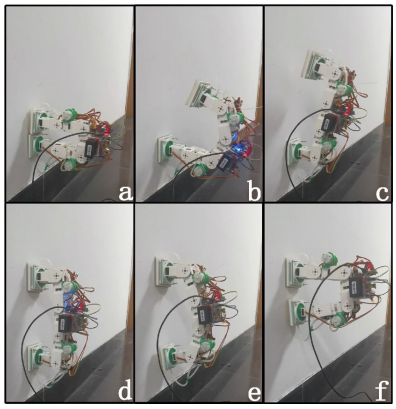

FIGURE 25. Motion process of robot on vertical wall surface.

moving on the vertical glass surface and wall in the videos of Supplementary Materials 3 and 4.

In order to verify the feasibility of the MPC-based bionic sucker controller to control the steering of the inchworm robot, we tested the steering motion of the robot on a horizontal metal material test bench, as shown in Fig.26. The test results show that the robot can complete the steering motion.

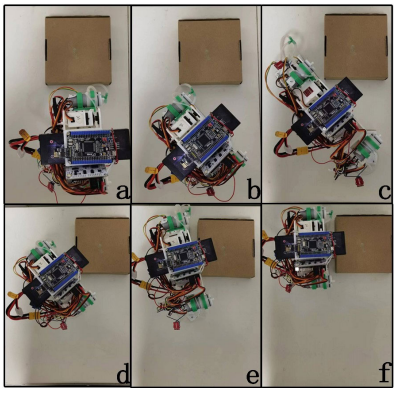

FIGURE 26. The process of robot steering motion.

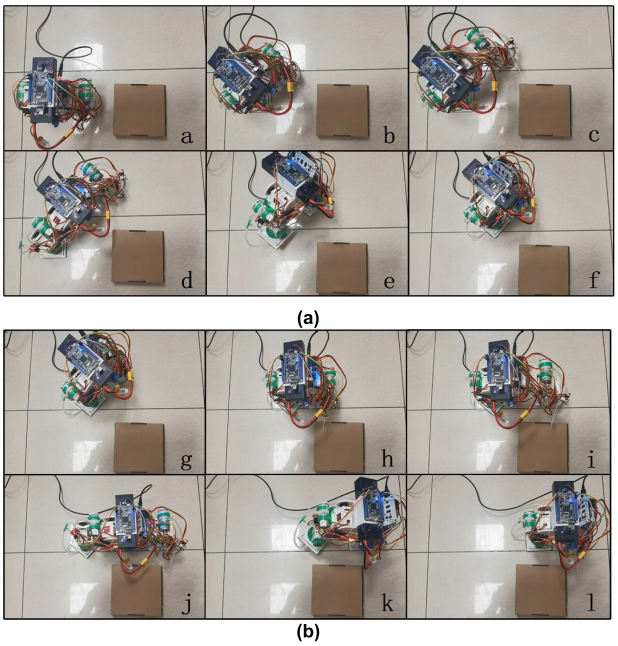

FIGURE 27. The motion process of combining step gait and turning gait of robots.

In order to verify the improvement of the walking and turning postures of the inchworm like robot on its motion ability, we combined the two postures to control the robot to complete the obstacle avoidance process, as shown in Figure 27. Figure 27 (a) shows the turning gait during the first half of the obstacle avoidance process, while Figure 27 (b) shows the step gait during the second half of the obstacle avoidance process. It can be seen that the step gait and turning gait we designed for the inchworm like robot can be combined with control to improve the robot's operational performance. You can see the turning gait and stride gait used by the robot during obstacle avoidance in the video of Supplementary Material 5.

In order to further test the motion performance of the robot, we selected a load-bearing column of an elevated bridge as the testing platform outdoors, with a surface made of cement material, which has a higher roughness compared to the previously tested plane. We control the robot to move vertically on this plane, as shown in Figure 28. The motion process can be seen in the video of Supplementary Material 10, where the robot is able to complete the step motion.

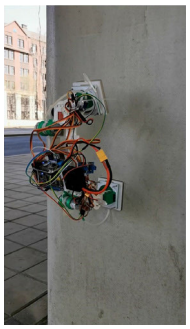

FIGURE 28. Robots perform stride gait on cement pillars.

In the video of Supplementary Material 6, you can see the continuous movement of the robot in the horizontal plane; In the video of Supplementary Material 7, you can see the continuous movement of the robot on the vertical metal door surface; In the video of Supplementary Material 8, you can see the continuous movement of the robot on the vertical glass surface; In the video of Supplementary Material 9, you can see the continuous movement of the robot on the wall.

V. CONCLUSION

In this paper, a motion control method of bionic sucker inchworm robot based on MPC is proposed. Firstly, an imitation octopus negative pressure sucker is designed and a sucker control model is proposed. Under negative pressure control, the adsorption pressure of the sucker can be adjusted to meet the needs of the trunk structure movement. Secondly, a bionic sucker controller based on MPC is designed, and the closed-loop control is realized by using the data feedback from the air pressure sensor. The MPC control algorithm adjusts the flow rate of the vacuum pump to adjust the adsorption force of the sucker. The algorithm collects the pressure data of the sucker to predict the future operating state and correct the output expectation of the flow rate variation of the vacuum pump. Then, a bionic sucker-type inchworm robot is designed. The designed bionic sucker is installed at the end of the inchworm robot as the tentacle of the robot. The torso structure of the inchworm robot is equipped with four longitudinal servo motors and two transverse servo motors, which can realize 'Ω' motion gait and steering gait. Thirdly, a motion gait based on MPC-BSC is proposed: 'Ω' motion gait and steering gait.

Finally, the adsorption force of the sucker on different material planes was tested experimentally. The adsorption forces on the metal plane, the wood plane, the glass plane, the ceramic tile plane and the wall surface were respectively; to verify the effectiveness of the MPC-based sucker controller, we use MATLAB to simulate the MPC-based bionic sucker

controller. The performance of vacuum pump flow rate control of PID control algorithm and MPC control algorithm is compared by simulation. The experimental results show that MPC control has faster response speed and higher stability. It is verified that the bionic sucker controller based on MPC can control the feasibility of the inchworm robot moving on different angle planes. The controller can control the robot to complete the movement gait on the glass plane, the tile plane and the wall surface, and realize the steering gait on the metal plane.

As a conceptual robot, the inchworm robot designed in this paper can be applied in different working environments by adjusting the size of the robot. In small size volume, it can detect the internal situation of narrow space; in large size, it is possible to transport items to places where conventional transport equipment cannot reach. There are still some shortcomings in the inchworm robot designed in this paper, such as the attitude planning of the sucker adsorption process, the optimization of the angle of the servo motor when the robot is stepping. These problems will be solved in the follow-up work.

REFERENCES

[1] H. Jiang, E. W. Hawkes, C. Fuller, M. A. Estrada, S. A. Suresh, N. Abcouwer, A. K. Han, S. Wang, C. J. Ploch, A. Parness, and M. R. Cutkosky, "A robotic device using gecko-inspired adhesives can grasp and manipulate large objects in microgravity," *Sci. Robot.*, vol. 2, no. 7, Jun. 2017, Art. no. eaan4545.

[2] B. Gamus, L. Salem, A. D. Gat, and Y. Or, "Understanding inchworm crawling for soft-robotics," *IEEE Robot. Autom. Lett.*, vol. 5, no. 2, pp. 1397–1404, Apr. 2020.

[3] M. Li, Z. Liu, M. Wang, G. Pang, and H. Zhang, "Design of a parallel quadruped robot based on a novel intelligent control system," *Appl. Sci.*, vol. 12, no. 9, p. 4358, Apr. 2022.

[4] H. Zhu, H. Zhang, L. Jiang, W. Wu, X. Zhang, X. Zhou, and Y. Guan, "Climbot: A bio-inspired modular biped climbing robot—System development, climbing gaits, and experiments," *J. Mech. Robot.*, vol. 8, no. 2, Jan. 2016, Art. no. 021026.

[5] J.-S. Koh and K.-J. Cho, "Omega-shaped inchworm-inspired crawling robot with large-index-and-pitch (LIP) SMA spring actuators," *IEEE/ASME Trans. Mechatronics*, vol. 18, no. 2, pp. 419–429, Apr. 2013.

[6] B. Gamus, A. D. Gat, and Y. Or, "Dynamic inchworm crawling: Performance analysis and optimization of a three-link robot," *IEEE Robot. Autom. Lett.*, vol. 6, no. 1, pp. 111–118, Jan. 2021.

[7] D. Zhang and D. Wang, "WALS-robot: A compact and transformable wheel-arm-leg-sucker hybrid robot," in *Proc. IEEE/RSJ Int. Conf. Intell. Robots Syst. (IROS)*, Oct. 2016, pp. 2584–2589.

[8] W. Huang, J. Xiao, F. Zeng, P. Lu, G. Lin, W. Hu, X. Lin, and Y. Wu, "A quadruped robot with three-dimensional flexible legs," *Sensors*, vol. 21, no. 14, p. 4907, Jul. 2021.

[9] H. Ko, H. Yi, and H. E. Jeong, "Wall and ceiling climbing quadruped robot with superior water repellency manufactured using 3D printing (UNIclimb)," *Int. J. Precis. Eng. Manuf.-Green Technol.*, vol. 4, no. 3, pp. 273–280, Jul. 2017.

[10] P. Ngamkajornwiwat, J. Homchanthanakul, P. Teerakittikul, and P. Manoonpong, "Bio-inspired adaptive locomotion control system for online adaptation of a walking robot on complex terrains," *IEEE Access*, vol. 8, pp. 91587–91602, 2020.

[11] A. Garcia, G. Krummel, and S. Priya, "Fundamental understanding of millipede morphology and locomotion dynamics," *Bioinspiration Biomimetics*, vol. 16, no. 2, Mar. 2021, Art. no. 026003.

[12] I. H. Han, H. Yi, C.-W. Song, H. E. Jeong, and S.-Y. Lee, "A miniaturized wall-climbing segment robot inspired by caterpillar locomotion," *Bioinspiration Biomimetics*, vol. 12, no. 4, Jun. 2017, Art. no. 046003.

[13] P. Chattopadhyay, A. Majumder, H. Dikshit, S. K. Ghoshal, and A. Maity, "A bio-inspired climbing robot: Design, simulation, and experiments," *IOP Conf. Ser., Mater. Sci. Eng.*, vol. 377, Jun. 2018, Art. no. 012105.

[14] S. Manzoor and Y. Choi, "Central patten generator based locomotion in inchworm robot," in *Proc. 11th Int. Conf. Ubiquitous Robots Ambient Intell. (URAI)*, Kuala Lumpur, Malaysia, Nov. 2014, pp. 419–422.

[15] F. Moreira, A. Abundis, M. Aguirre, J. Castillo, and P. A. Bhounsule, "An inchworm-inspired robot based on modular body, electronics and passive friction pads performing the two-anchor crawl gait," *J. Bionic Eng.*, vol. 15, no. 5, pp. 820–826, Sep. 2018.

[16] Z. Shi, J. Pan, J. Tian, H. Huang, Y. Jiang, and S. Zeng, "An inchworm-inspired crawling robot," *J. Bionic Eng.*, vol. 16, no. 4, pp. 582–592, Jul. 2019.

[17] D. Xie, J. Liu, R. Kang, and S. Zuo, "Fully 3D-printed modular pipe-climbing robot," *IEEE Robot. Autom. Lett.*, vol. 6, no. 2, pp. 462–469, Apr. 2021.

[18] S. Liu, F. Wang, Z. Liu, W. Zhang, Y. Tian, and D. Zhang, "A two-finger soft-robotic gripper with enveloping and pinching grasping modes," *IEEE/ASME Trans. Mechatronics*, vol. 26, no. 1, pp. 146–155, Feb. 2021.

[19] S. Rozen-Levy, W. Messner, and B. A. Trimmer, "The design and development of branch bot: A branch-crawling, caterpillar-inspired, soft robot," *Int. J. Robot. Res.*, vol. 40, no. 1, pp. 24–36, Jan. 2021.

[20] Y. Wang, Q. Du, T. Zhang, and C. Xue, "The WL_PCR: A planning for ground-to-pole transition of wheeled-legged pole-climbing robots," *Robotics*, vol. 10, no. 3, p. 96, Jul. 2021.

[21] T. Bandyopadhyay, R. Steindl, F. Talbot, N. Kottege, R. Dungavell, B. Wood, J. Barker, K. Hoehn, and A. Elfes, "Magneto: A versatile multi-limbed inspection robot," in *Proc. IEEE/RSJ Int. Conf. Intell. Robots Syst. (IROS)*, Oct. 2018, pp. 2253–2260.

[22] M. B. Khan, T. Chuthong, J. Homchanthanakul, and P. Manoonpong, "Electromagnetic feet with soft toes for adaptive, versatile, and stable locomotion of an inchworm-inspired pipe crawling robot," *Frontiers Bioeng. Biotechnol.*, vol. 10, Feb. 2022, Art. no. 842816.

[23] B. He, Z. Wang, M. Li, K. Wang, R. Shen, and S. Hu, "Wet adhesion inspired bionic climbing robot," *IEEE/ASME Trans. Mechatronics*, vol. 19, no. 1, pp. 312–320, Feb. 2014.

[24] Z. Yu, Y. Shi, J. Xie, S. X. Yang, and Z. Dai, "Design and analysis of a bionic adhesive foot for gecko robot climbing the ceiling," *Int. J. Robot. Autom.*, vol. 33, no. 4, Jul. 2018, pp. 1–10.

[25] Z. Xie, A. G. Domel, N. An, C. Green, Z. Gong, T. Wang, E. M. Knubben, J. C. Weaver, K. Bertoldi, and L. Wen, "Octopus arm-inspired tapered soft actuators with suckers for improved grasping," *Soft Robot.*, vol. 7, no. 5, pp. 639–648, Oct. 2020.

[26] R. H. Plaut, "Mathematical model of inchworm locomotion," *Int. J. Non-Linear Mech.*, vol. 76, pp. 56–63, Nov. 2015.

[27] J. Zhang, T. Wang, J. Wang, B. Li, J. Hong, J. X. J. Zhang, and M. Y. Wang, "Dynamic modeling and simulation of inchworm movement towards bio-inspired soft robot design," *Bioinspiration Biomimetics*, vol. 14, no. 6, Sep. 2019, Art. no. 066012.

[28] S. Sareh, K. Althoefer, M. Li, Y. Noh, F. Tramacere, P. Sareh, B. Mazzolai, and M. Kovac, "Anchoring like octopus: Biologically inspired soft artificial sucker," *J. Roy. Soc. Interface*, vol. 14, no. 135, Oct. 2017, Art. no. 20170395.

[29] M. B. Khan, T. Chuthong, C. Danh Do, M. Thor, P. Billeschou, J. C. Larsen, and P. Manoonpong, "ICrawl: An inchworm-inspired crawling robot," *IEEE Access*, vol. 8, pp. 200655–200668, 2020.

[30] S. D. de Rivaz, B. Goldberg, N. Doshi, K. Jayaram, J. Zhou, and R. J. Wood, "Inverted and vertical climbing of a quadrupedal microrobot using electroadhesion," *Sci. Robot.*, vol. 3, no. 25, Dec. 2018, Art. no. eaau3038.

[31] J. Cao, W. Liang, Y. Wang, H. P. Lee, J. Zhu, and Q. Ren, "Control of a soft inchworm robot with environment adaptation," *IEEE Trans. Ind. Electron.*, vol. 67, no. 5, pp. 3809–3818, May 2020.

[32] H. Bagheri, A. Hu, S. Cummings, C. Roy, R. Casleton, A. Wan, N. Erjavic, S. Berman, M. M. Peet, D. M. Aukes, X. He, S. C. Pratt, R. E. Fisher, and H. Marvi, "New insights on the control and function of octopus suckers," *Adv. Intell. Syst.*, vol. 2, no. 6, Jun. 2020, Art. no. 1900154.

[33] L. Fang-Hua, Z. Jian-Wu, and C. Dan, "Research on path planning of driverless vehicle based on improved MPC," *Southern Agricult. Machinery*, vol. 53, no. 11, pp. 42–44, 2022.

[34] W. Yu-Liang, L. Han-Qing, and C. Zhao-Ying, "Research on the control system of unmanned rice transplanter based on MPC algorithm," *Res. Agricult. Mechanization*, vol. 45, no. 3, pp. 106–112, 2023.
[35] C. Zhen, Z. Lu-Yang, and Z. Zhi-Qiang, "MPC based trajectory tracking algorithm for unmanned vehicles," *Practical Automot. Technol.*, vol. 47, no. 21, pp. 43–46, 2022.
[36] X. Xian-Yi, W. Yu-Han, and J. Lisheng, "MPC trajectory tracking control based on changing control time step," *J. Jilin Univ.*, pp. 1–10, 2023.

CHENGZE XUE was born in Tianjin, China, in 1996. He received the bachelor's degree majored in electronic information engineering from Jilin University, Jilin, in 2019, where he is currently pursuing the Master of Engineering degree in circuits and systems. His research interests include robot control and embedded applications.

QIAOLING DU received the Ph.D. degree from Jilin University, in 2009. She is currently an Associate Professor with the College of Electronic Science and Engineering, Jilin University. Her research interests include wireless sensor network positioning technology, robot path planning and navigation, and water quality monitoring systems.

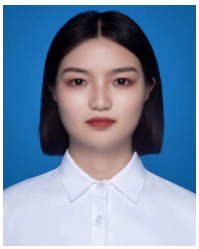

WENLI MA was born in March 1996. She received the degree in detection technology from Shijiazhuang Railway University, in 2022, and the master's degree in automation equipment. She is currently pursuing the Ph.D. degree in circuit and system engineering with Jilin University. Her research interest includes robot motion control.

YINFENG GENG was born in Changchun, China, in 2000. He received the bachelor's degree majored in electronic information engineering from Jilin University, Jilin, in 2022, where he is currently pursuing the master's degree in electrical circuits and systems. His research interests include robot control and embedded applications.